Planetary and Space Science 58 (2010) 1207–1214

Contents lists available at ScienceDirect

Planetary and Space Science

journal homepage: www.elsevier.com/locate/pss

Concatenation of HRSC colour and OMEGA data for the determination and 3D-parameterization of high-altitude CO_2 clouds in the Martian atmosphere

Frank Scholten [a], Harald Hoffmann [a,*], Anni Määttänen [b], Franck Montmessin [b], Brigitte Gondet [c], Ernst Hauber [a]

[a] Deutsches Zentrum für Luft- und Raumfahrt (DLR), Institute of Planetary Research, Rutherfordstrasse 2, 12489 Berlin, Germany
[b] Laboratoire Atmosphères, Milieux, Observations Spatiales, CNRS/IPSL/UVSQ/UPMC, BP 3, Guyancourt 78280, France
[c] Institut d'Astrophysique Spatiale (IAS), Orsay 91405, France

ARTICLE INFO

Article history:
Received 15 July 2009
Received in revised form
25 February 2010
Accepted 20 April 2010
Available online 27 April 2010

Keywords:
Mars
Atmosphere
Clouds
Carbon dioxide

ABSTRACT

We used Mars Express HRSC and OMEGA data to investigate mesospheric cloud features observed in the equatorial belt of Mars from December 2007 until early March 2008. This period corresponds to early northern spring of Martian year 29. The reflection peak at 4.26 μm in OMEGA data identifies the clouds as CO_2 ice clouds. HRSC observed the clouds together with OMEGA in five orbits. Cloud features are most prominent in the shortwave HRSC colour channels with wavelength centers at 440 and 530 nm, but rarely visible in all other channels. In the period of Ls 0–36°, OMEGA and HRSC together detected mesospheric CO_2 ice clouds in 40 orbits. They occur in a latitude belt of $\pm 20°$ around the equator and at longitudes between 240°E (Tharsis) in the West and 30°E (Sinus Meridiani) in the East. The clouds were observed between 3 and 5 p.m. local time with mainly ripple-like to filamentary cloud forms. The viewing angles of the HRSC blue and green colour channels differ by 6.6° and the resulting parallax can be used to directly measure cloud heights by means of ray intersection. 17 HRSC data takes were found to exhibit clouds with heights from 66 to 83 km with an accuracy of 1–2 km. The pushbroom imaging technique also yields a time delay for the two observations in the order of 5–15 s close to periapsis, and therefore time-related cloud movements can be detected. A method was developed to determine the across-track cloud displacements, which can directly be translated to wind velocities. Zonal cloud movements could be measured in 13 cases and were oriented from East to West. Related wind speeds range between 60 and 93 m/s with an accuracy of 10–13 m/s.

1. Introduction

CO_2 is the main constituent of the Martian atmosphere and its seasonal cycle has an important role for atmospheric dynamics and the Martian climate. Most prominent is the formation of the polar CO_2 frost deposits that accounts for seasonal surface pressure variations of $>30\%$. The condensation of CO_2 ice occurs at temperatures around 145 K (at 6 mbar) and may result in the formation of frost directly on the surface or of CO_2 ice clouds (e.g. James et al., 1992). The importance of precipitation for the generation of the polar frost cap, however, is poorly understood. Conditions to exceed the CO_2 saturation level can only be reached at the winter polar night and in the mesosphere (Montmessin et al., 2006; Colaprete et al., 2008). Most clouds known to occur in planetary atmospheres originate from the condensation of minor constituents of the atmospheres. The peculiar situation of CO_2 cloud formation within the bulk CO_2 atmosphere results in many unknowns for the understanding and modelling of processes involved. Heterogeneous or homogeneous nucleation could be involved in the condensation. The mesospheric clouds were not predicted by the General Circulation Models (e.g., Forget et al., 1999), which implies insufficient process description or an important effect of subgrid-scale phenomena in the cloud formation process. The mesospheric CO_2 cloud observations will help to better constrain the models and their subsequent development.

Cloud echoes detected by the Mars Orbiter Laser Altimeter (MOLA) onboard Mars Global Surveyor (MGS) at both poles at altitudes below 20 km during polar night have been interpreted indirectly as CO_2 ice clouds (Pettengill and Ford, 2000; Ivanov and Muhleman, 2001) consistent with the very cold surface temperatures (James et al., 1992). The first spectroscopic identification of CO_2 aerosols in the atmosphere at an altitude of about 80 km was obtained by the Planetary Fourier Spectrometer (PFS) onboard Mars Express (MEx) during a limb observation (Formisano et al., 2006). Indirect evidence for high-altitude CO_2 clouds was

* Corresponding author. Tel.: +49 30 67055327; fax: +49 30 67055402.
E-mail address: harald.hoffmann@dlr.de (H. Hoffmann).

0032-0633/$ - see front matter © 2010 Elsevier Ltd. All rights reserved.
doi:10.1016/j.pss.2010.04.015

provided by star occultation measurements of the MEx SPICAM instrument (Montmessin et al., 2006) and the combined analysis of MGS limb observations with MOC and TES (Clancy et al., 2007). Temperature retrievals of the SPICAM occultation data (Montmessin et al., 2006; Forget et al., 2009) as well as of MGS TES and radio science observations (Colaprete et al., 2008) indicate that CO_2 supersaturation may occur within very cold pockets of the mesosphere. In situ measurements of extremely cold temperatures within the Martian mesosphere have been obtained during the Pathfinder atmospheric entry and descent (Schofield et al., 1997). Based on these measurements and earth-based microwave observations Clancy and Sandor (1998) proposed the probable occurrence of CO_2 clouds at altitudes from 70 to 80 km.

Recently, the MEx OMEGA imaging spectrometer reported on 19 detections of mesospheric CO_2 ice clouds at low- to mid-latitudes (Montmessin et al., 2007). Atmospheric CO_2 ice could be identified in nadir observations based on the reflectance peak at 4.24–4.26 μm due to resonant scattering of photons, which is correlated with a brightening at wavelengths <0.7 μm. Shadow measurements in two cases yield a cloud altitude of about 80 km and an effective aerosol particle size of 1.5 μm. Spectral modelling revealed that the minimum particle size should be at least 0.2 μm and that CO_2 ice clouds are only detectable at altitudes above 30 km.

We present new observations of mesospheric equatorial CO_2 ice clouds obtained by the High Resolution Stereo Camera experiment (HRSC, Jaumann et al., 2007) and by the OMEGA imaging spectrometer onboard Mars Express (Bibring et al., 2004) from December 2007 until March 2008 which corresponds to early Northern spring of the Martian year 29. Special emphasis will be given to describe methodological aspects and accuracies involved in the determination of CO_2 ice cloud heights and velocities. Since the along-track pushbroom stereo design of HRSC allows for high-resolution 3D measurements, the retrieval of specific geometric cloud properties, e.g. cloud altitude and velocity, became a concrete subject of interest. The typical application of the HRSC stereo capability is the derivation of high-resolution digital terrain models from multi-stereo data provided by the HRSC panchromatic stereo channels (Scholten et al., 2005; Gwinner et al., 2009a). Because of their spectral reflectivity and scattering properties CO_2 ice clouds appear, if at all, only faint in broad-band panchromatic channels. But the HRSC short-wave bands (green and blue) show features, which obviously correspond to CO_2 ice clouds in the Martian atmosphere as spectrally identified by OMEGA in simultaneous observations (Fig. 1). The HRSC stereo angle between the blue and green colour bands is small as compared to the panchromatic surface stereo. Nevertheless, the derivation of the altitude of some cloud features appears to be reasonable to at least some extent. Additionally, it can be expected, that the time delay between the observations in both channels allows for the assessment of zonal velocity parameters.

2. HRSC, OMEGA and observational constraints

2.1. HRSC imaging geometry for CO_2 ice cloud parameterization

The HRSC provides multiple-stereo capability by data acquisition with the pushbroom principle with 9 different CCD arrays, each with 5184 active pixels, placed in the focal plane (focal length 175 mm) at different positions behind one single optics (Neukum et al., 2004; Jaumann et al., 2007). The across-track field of view (FOV) is 11.9° yielding a swath width of 63 km from 300 km altitude. Five of the sensors are equipped with panchromatic filters (675 ± 90 nm) for stereo imaging and are oriented in nadir, $\pm18.9°$ and $\pm12.8°$ out of nadir in the along-track direction. Four additional spectral bands provide information at near-infrared (970 ± 45 nm), red (750 ± 20 nm), green (530 ± 45 nm), and blue (440 ± 45 nm) wavelengths. While the red and near-infrared sensors are placed at $\pm15.9°$, the blue and green channels are only marginally off-nadir at $\pm3.3°$ (cp. Fig. 2). In either case, any measurement of the same stationary feature in at least two different sensors allows for the derivation of spatial information of this feature. Using the geometric camera calibration data the measurements of image coordinates of an identical feature can be transformed to camera-internal lines of sight. These rays can be transformed to rays within the Mars-fixed coordinate system using the actual orientation of the camera (derived from nominal MEx orbit/pointing and HRSC alignment) at the respective imaging times. The intersection point of these rays defines the lateral and vertical location of the feature within the Mars coordinate system.

Cloud features, rather than the solid Martian surface, have to be expected to vary in time and to move to some extent. The pushbroom imaging technique with the slight forward and backward looking tilt of the short-wave HRSC bands will result in a time delay between the two measurements of an identical feature. Time differences close to periapsis are typically in the order of 5–15 s for objects at an altitude of 60–70 km. Movements

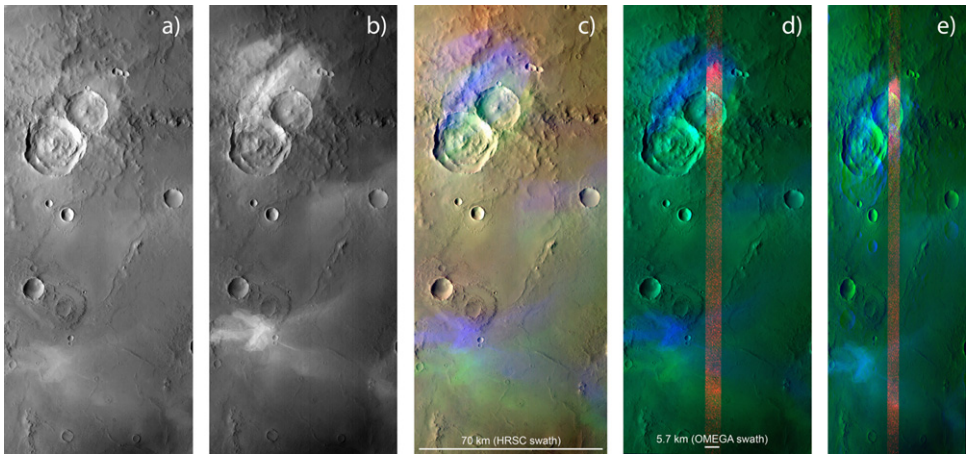

Fig. 1. Mars Express orbit 5141, Arabia Terra (Ls=11.9°, 16:30 local time). (a) HRSC green band image; (b) HRSC blue band image; (c) RGB colour composite with the HRSC red, green and blue band images, rectified to Mars IAU ellipsoid; (d) RGB composite: OMEGA, 4.24 μm (red), HRSC green band (green), HRSC blue band (blue) rectified to Mars IAU ellipsoid; (e) RGB composite as in (d) but rectified to 83 km ellipsoidal altitude (i.e. the measured cloud altitude). All images contrast enhanced.

along the MEx near-polar orbit plane (in meridional direction, North/South) will then falsify the derived vertical coordinate (altitude) of the cloud feature. Zonal (East/West) across-orbit movements will cause the rays defined by the stereo observations to be apart from another and not to intersect perfectly. This parallax across the stereo direction will not influence the calculated altitude itself, only the nominal accuracy of the derived altitude will be degraded. But, as a by-product, the parallax yields the actual displacement (cp. Fig. 3) of the cloud during the observation which is a measure of the zonal wind velocity.

2.2. OMEGA imaging spectrometer

The MEx OMEGA instrument is an imaging spectrometer covering the wavelength range 0.38–5.1 μm with 352 spectral samples, 7–20 nm wide (Bibring et al., 2004, 2005). It comprises two co-aligned channels from 0.38 to 1.05 μm and from 0.93 to 5.1 μm, respectively. A CCD area array detector is used in the visible to near-infrared gathering data in a pushbroom mode. The infrared channel is operated in a whiskbroom mode with a scanning mirror in front of the telescope to achieve across-track coverage. A maximum number of 128 pixels can be acquired across-track yielding a total FOV of 8.8° which is used from high spacecraft altitudes. Close to periapsis, the OMEGA swath consists of 16 pixels or 1.1° in order to cope with the high spacecraft velocity.

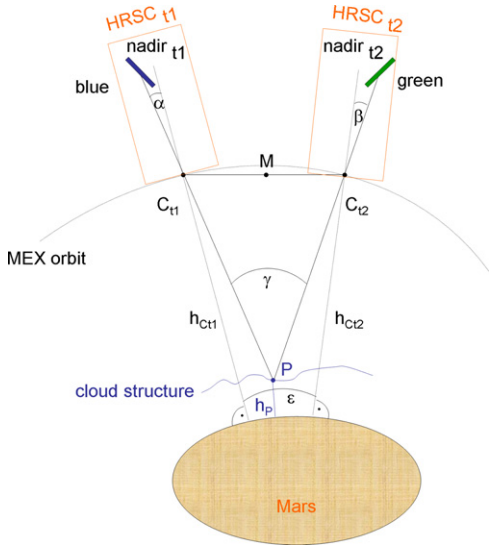

Fig. 2. HRSC along-track stereo geometry for cloud height measurements with the blue and green channels, both 3.3° out-of-nadir.

2.3. Observational constraints

MEx has a highly elliptical and almost polar orbit with an inclination of 86.7° and a periapsis altitude close to 300 km. The sub-periapsis point precedes in latitude by about 0.17° from orbit to orbit while the local time at periapsis shifts by about 40 s. The orbit characteristics and the different observation strategies of both instruments have quite some impact on the opportunities to image carbon dioxide clouds.

OMEGA normally uses the maximum duration for a nadir pointing that is allowed by spacecraft resources and a typical OMEGA observation lasts from 40 up to 65 min around periapsis. This is sufficient to observe a latitudinal range of up to 180° if feasible from an illumination point of view. Hence, OMEGA is well suited to monitor atmospheric dynamic phenomena during daytime conditions over a broad latitudinal range. HRSC, instead, is aiming to map the Martian surface at high spatial resolution and in stereo. Consequently, it is operated mostly close to periapsis. A typical image data acquisition lasts only for a few to some 10 min due to data volume restrictions. Latitudinal coverage within a given time period is, therefore, limited.

Late December 2007, the MEx sub-periapsis point was crossing the equator while preceding towards the North during northern spring, a season with frequent mesospheric cloud detections in the equatorial belt in previous Martian years (Montmessin et al., 2007; Clancy et al., 2007). Moreover, MEx performed some manoeuvres to change its orbit from an 11/3- to an 18/5-resonance in November and December 2007, i.e. MEx sub-periapsis point returns to the same geographic location with a slight westward offset of about 0.9° in longitude after 18 orbits, which corresponds to 5 Martian days. Thus, the longitudinal coverage was improved with 18 observable regions about 20° in longitude apart from each other as compared to the former 11 longitudinal regions. Before the manoeuvres, OMEGA and HRSC had a break in their observations with the sub-periapsis point being in the dark. Both instruments resumed operations on 6 December 2007 at Ls=358°. 3 months later and due to the periapsis drift, HRSC was imaging mainly at mid-northern latitudes and outside the equatorial belt. Our analysis will, therefore, focus on observations from December 2007 until early March 2008 covering MEx orbits 5044–5370 during early northern spring (Ls 358–42°) of the Martian year 29.

3. Stereo methodology and accuracy assessment for HRSC cloud altitude and velocity measurements

Typical exploitation of the stereo capability makes use of automated image matching procedures applied to stereo image data of the solid surface of bodies. Area-based matching, as applied in Scholten et al. (2005) and Gwinner et al. (2009a), depends on the uninterrupted representation of the respective

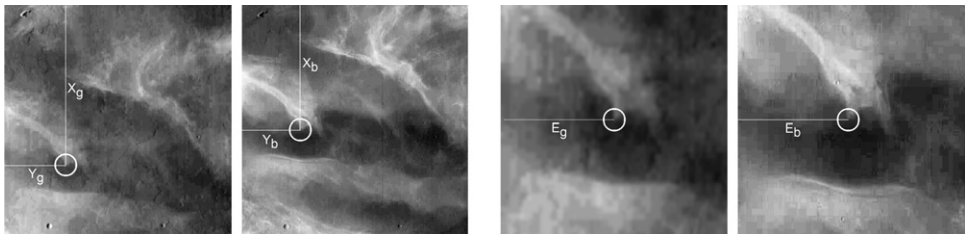

Fig. 3. Measurement example in MEx orbit 5117, Tharsis (Ls=8.5°, 16:42 local time): Left: definition of *x*, *y* raw image coordinates in both HRSC band images for altitude determination by forward ray intersection. Right: definition of eastward parallax in map-projected HRSC images, rectified to the feature altitude, for velocity determination by relating the parallax to the time delay between the bands.

surface within the involved imagery. The diffuse character of clouds does not meet this requirement. Automated feature-based matching would also fail or yield erroneous results in case of diffuse structures. In order to achieve a maximum of reliability and to minimize measurement errors, we only use visual interpretation and manual measurements for the definition of identical cloud features in different images. Only those identical features within cloud structures that can be identified beyond doubt in the different images are selected as input for the following altitude and velocity calculations. The decrease of number of features that meet these requirements is not critical, since we primarily focus on the determination of general cloud attributes, rather than on their structural assembly. The geometrical configuration for cloud altitude and velocity measurements by stereo from HRSC stereo information (green and blue channels) is sketched in Fig. 2. In the following we discuss the theoretical accuracy.

The achievable accuracy for altitude and velocity measurements of cloud features depends on the following:

- the imaging geometry,
- the point measurement accuracy,
- the accuracy of required orientation data, and
- the movement direction of the cloud features.

Cloud features are imaged in the HRSC blue and green channels from two different camera positions C_{t1} and C_{t2} at two different times $t1$ and $t2$, respectively (cp. Fig. 2). Along its elliptical orbit the MEx spacecraft and thus the fix-mounted HRSC is typically oriented towards nadir for imaging. The HRSC blue and green channels are placed $\pm 3.3^\circ$ off-nadir. As mentioned before, the calculation of the coordinates (latitude, longitude, and altitude) of a cloud feature P in the Mars-fixed coordinate frame is performed by forward ray intersection of both lines of sight, which are defined by the camera calibration (CCD pixel positions and focal length) and the exterior orientation data (orbit position and pointing at the respective times t1 and t2).

For the assessment of the accuracy (error budget) for the altitude calculation we can simplify the geometry by using the triangles C_{t1}PM and C_{t2}PM:

$$h_P = h_C\text{-}d$$

where h_P is the altitude of the cloud feature, h_C the altitude of the MEx orbit $(h_C = h_{C_{t1}}\text{-}h_{C_{t2}})$, d the distance PM.

Within each triangle we have $b/2 = d \tan(\gamma/2)$, and we obtain

$$h_P = h_C - b/(2\tan(\gamma/2))$$

where b is the distance $C_{t1}C_{t2}$ and γ is the effective stereo angle.

Now we have to check for the accuracies of the relevant parameters h_C, b, γ within this equation and their influence on the altitude calculation. The accuracy of the knowledge of the reconstructed MEx orbit σ_{h_c} is approx. 0.1–0.2 km for the altitude (Gwinner et al., 2009b). This value directly contributes to the final cloud altitude accuracy.

Because of the curvature of the MEx orbit, the effective stereo angle γ is defined by

$$\gamma = \alpha + \beta + \varepsilon = 6.6^\circ + \varepsilon$$

The convergence angle ε (see Fig. 2) is variable with the distance d of the cloud feature P to the MEx orbit. Using a 300 km orbit altitude above the Mars ellipsoid for typical near-periapsis observations and assuming cloud heights between 60 and 70 km, b is 28–26 km, and ε is 0.5–0.4°. Thus, the worst (minimum) effective stereo angle γ is $6.6^\circ + 0.4^\circ = 7.0^\circ$.

The error contribution σ_γ of the stereo angle γ is determined by the accuracy of the viewing directions. It consists of residual geometrical calibration errors and of the uncertainty of the exterior orientation (pointing knowledge). Calibration is accurate to better than one IFOV ($< 0.002^\circ$). Relative pointing knowledge within the short imaging duration of t1–t2 is accurate to the same extent, but can exceed this up to 0.01° in case of high-frequent angular spacecraft movements (see Gwinner et al., 2009b). Within our stereo configuration a worst case orientation error of 0.01° contributes to the altitude accuracy with $\sigma_\gamma = 0.7$ km.

The last error component is the accuracy σ_b of the stereo base b. It is defined by the along-track position accuracy and is mainly affected by the visual identification and manual measurement accuracy of identical cloud features within the two images. While most of the cloud structures within the HRSC images are rather diffuse or smeared, some features can be identified and measured with an accuracy of 1 image pixel. MEx HRSC colour images are typically captured with 4×4 or 8×8 macropixel binning. Therefore, near-periapsis images with a nominal resolution of approx. 10–18 m/pixel (1×1) comprise 40–150 m/pixel for the green and blue bands. A 1 pixel measurement accuracy contributes to the accuracy of the stereo base and finally to the altitude accuracy with $\sigma_b = 0.3$–1.2 km.

The error influence from the knowledge of the along-orbit position component can be neglected, since the accuracy for the difference between two positions can be expected to be far better than 0.1 km, because the MEx orbit follows well enough Kepler's rules for objects in planetary orbits.

Now we can derive the error propagation for altitude calculations by

$$\sigma_{h_P} = (\sigma_{h_c}^2 + \sigma_\gamma^2 + \sigma_b^2)^{1/2} = ((0.2\,\text{km})^2 + (0.7\,\text{km})^2 + (0.3\text{–}1.2\,\text{km})^2)^{1/2} = +/-0.8\text{–}1.4\,\text{km}$$

Finally, we have to take into account the influence of the movement direction of cloud features to the calculation of their altitude, since along-track movements and apparent height parallaxes are directly correlated. The time delay between blue and green near-periapsis imaging of a feature at 70 km altitude is about 5–15 s. For each multiple of 10 m/s along-track (meridional) movement we get an influence of 50–150 m to the apparent stereo base. This relates to an additional error contribution to the calculated altitude of about 0.4–1.2 km for each 10 m/s along-track (meridional) movement.

In total the theoretical value for the absolute accuracy of altitude measurements near periapsis can be estimated by ± 1 km. This value has to be extended to $\pm$ 2–3 km, if meridional movements of up to 10–15 m/s cannot be excluded. Meridional wind velocities in the order of a few ten m/s seem to be realistic. While direct measurements are not available, the gravity wave modelling approach by Joshi et al. (1995) yields maximum meridional wind speeds below 50 m/s.

The accuracy for zonal (across-track) movements of cloud features is determined by the apparent East–West parallax in geometrically corrected images, map projected to the previously determined altitude. This parallax can also be measured with 1 pixel accuracy (σ_P, 40–150 m near periapsis). Orientation angle errors (σ_O) of up to 0.01° contribute with an additional uncertainty of about 50 m. With the typical time delay of 5–15 s between the blue and green channel we have a total accuracy value σ_{Vz} for zonal movement velocities of

$$\sigma_{Vz} = 1/(5\text{–}15\,\text{s})(\sigma_P^2 + \sigma_O^2)^{1/2} = 1/(5\text{–}15\,\text{s})((0.04\text{–}0.15\,\text{km})^2 + (0.05\,\text{km})^2)^{1/2} = +/-13\text{–}10\,\text{m/s}$$

An exemplary measurement of a cloud feature in the HRSC green and blue bands is shown in Fig. 3.

4. CO_2 ice cloud detection and parameterization

Based on the characteristic Fresnel reflection peak at 4.26 μm (Montmessin et al., 2007), OMEGA detected CO_2 ice clouds in 28 orbits from December 2007 to early March 2008 (Määttänen et al., submitted for publication). The first detection was above Sinus Meridiani in MEx orbit 5062 at spring equinox (Ls = 0.8°). HRSC was operating in parallel with OMEGA in five of these orbits and exhibits unique signature in its map-projected colour data when observing the mesospheric clouds identified spectrally by OMEGA to consist of CO_2 ice crystals (Fig. 1). The clouds are most prominent in the HRSC blue band and less pronounced in the green band. In the red as well as in the panchromatic bands, the cloud features are rather weak and diffuse if visible at all while in the near-infrared band, the clouds have mostly vanished. This is consistent with the observed brightening in OMEGA data at wavelengths shortward of 0.7 μm. In standard map-projected HRSC RGB colour images (Scholten et al., 2005), the features appear twice and in different colours. This effect is caused by the uncorrected parallax of the cloud being high above the Martian surface and disappears if map-projected to the measured cloud altitude. The spectral behaviour as observed in the HRSC colour channels is typical for condensate clouds. It is not possible to unequivocally determine the occurrence of atmospheric CO_2 ice from HRSC data alone and H_2O ice clouds cannot be excluded. Martian mesospheric water ice clouds have been reported (e.g., McConnochie and Smith, 2008; Fedorova et al., 2009), but were found at different seasons. The presence of discrete water ice clouds at altitudes above 50 km in northern spring seems rather unlikely since water condensation in lower altitudes should effectively limit the access of water vapour above 30 km (Clancy et al., 1996; Rodin et al., 1997). Based on the good correlation with the OMEGA observations we conclude that the mesospheric cloud features found only in HRSC data constitute CO_2 ice clouds.

4.1. Cloud altitude and velocity measurements in HRSC imagery

We have surveyed all HRSC images acquired in the aforementioned period (December 2007–February 2008). HRSC was engaged in 219 orbits and encountered mesospheric clouds in 17 orbits with a first occurrence in orbit 5109 at Ls = 7.4° and the last detection in orbit 5279 at Ls = 30.3°. Due to MEx orbital constraints, local times of the cloud features measured in HRSC data cover a range of about 2 h from 4:48 to 3:06 p.m. during the observational period of 3 months. Table 1 gives an overview of the results. Cloud and ground altitudes are given above the Mars IAU ellipsoid. Orbits marked with "*" provide parallel observations of HRSC and OMEGA described above. All other measurements rely to CO_2-like phenomena, found in HRSC, when OMEGA was not operating. Not listed in Table 1 is an HRSC blue channel observation of lineated cloud features in orbit 5170, when OMEGA was identifying simultaneously the occurrence of CO_2 ice clouds (Määttänen et al., submitted for publication). Problems during earth communications resulted in a loss of image data for this specific HRSC observation and the retrieval of cloud altitude or velocity is not feasible.

The cloud altitudes of all orbits range from 66.4 to 83.2 km with a mean of 75 km and are in good agreement with the cloud altitudes derived by Montmessin et al. (2007) with shadow measurements in OMEGA data. This corresponds to an altitude range of 65.8–83.4 km above the surface if we take local topography into account. As discussed earlier, absolute results for the altitude might be systematically offset 0.4–1.2 km for each 10 m/s along-track (meridional) movement.

Some orbits provide more than one measurement. In these cases we listed the mean of the altitudes, its error, and the standard deviation of the single measurements. The standard deviations of most orbits coincide quite well with the theoretical values for single measurements, previously estimated to be about 0.8–1.4 km. Some orbits (5134 and 5201) show significantly higher standard deviations (4.3 km), which might result from local vertical structures within the cloud formations.

The average East–West velocity component of 13 orbits is 73 m/s. The predominance of a westward cloud movement is related to the existence of strong easterly winds in the equatorial areas at these altitudes, where the cloud movement should reflect the wind speed and direction. In 4 cases, cloud features were too faint to allow for reliable across-track velocity measurements at all (marked with "–" in Table 1), while altitude determination by along-track stereo remains reasonable. Hence, the data base for velocity measurements is quite limited. Therefore we do not specify any measurement accuracy, but the range of 60–93 m/s indicates that the theoretical accuracy of 10–13 m/s comply with our velocity measurements. The HRSC wind measurements provide a rare dataset from the mesosphere that can be used to validate and constrain global climate models. Model predictions for zonal winds by the LMD GCM (Forget et al., 1999; Angelats i Coll et al., 2005) compare rather well with the HRSC observations with the slight tendency of underestimating the velocities. This may be explained by an overestimation of the temperatures in the mesosphere as described by Forget et al. (2009) based on SPICAM stellar occultation measurements. A detailed comparison with the LMD GCM will be performed elsewhere.

Mesospheric cloud altitude and direct cloud velocity measurements have been reported for equatorial clouds by McConnochie et al. (2005, submitted for publication) and Inada et al. (2007) based on observations with the Mars Odyssey Thermal Emission Imaging System (THEMIS). The THEMIS-VIS colour channels apply a push-frame imaging technique (McConnochie et al., 2006) which results in a rather small time-delay and parallax offset between the colour channel images. To derive cloud altitudes and velocities the mismatch between the colour images is minimized iteratively by reprojecting the data to different altitudes and by maximizing the correlation within a selected cloud feature (McConnochie et al., 2005, submitted for publication). Ray intersection calculations as presented here for the HRSC data compare rather well with one THEMIS observation described during early northern spring close to the equator (Ls 26°, 1°N, 262°E; McConnochie et al., submitted for publication) at an altitude of 74 ± 2 km and a westward cloud movement of 90 ± 20 m/s.

To our knowledge, the THEMIS and the HRSC observations are the only direct wind velocity measurements of mesospheric clouds until now. Most of our information on wind velocities in the Martian middle atmosphere have been obtained by ground based observations in the microwave range (e.g. Lellouch et al., 1991; Clancy and Sandor, 1998; Moreno et al., 2009) and quite recently, in the infrared at about 10 μm by heterodyne spectroscopy (Sonnabend et al., 2006, 2008). These earth-based observations, however, are probing different altitudes by measuring zonal winds around 50 km and at completely different scales. The observed dominant wind direction close to the equator, however, concurs with the HRSC measurements and wind velocities between 60 and 90 m/s are quite common.

4.2. Mesospheric cloud forms

Thanks to the large swath width especially close to periapsis and the high spatial resolution, HRSC images provide a good

Table 1
HRSC cloud feature observations and measurements in the blue and green bands (*simultaneous observation by OMEGA).

MEx orbit number	Mean cloud alt. (km)	Number of features	Error of mean alt. (km)	Standard deviation (km)	E→W velocity (m/s)	Northern latitude (deg.)	Eastern longitude (deg.)	Ground alt. (km)	Local time	Ls [°]
5109	68.1	1	–	–	68	2.4	347.1	−3.9	16:48	7.4
5117	79.2	7	0.8	2.0	63	0.8	265.9	4.0	16:42	8.5
5134	76.4	3	2.5	4.3	73	11.9	4.8	−2.3	16:30	10.8
5135	79.8	3	0.3	0.5	93	2.1	265.0	4.6	16:30	11.0
5141*	83.2	2	0.8	1.1	66	7.1	24.8	−0.2	16:30	11.8
5146*	79.2	1	–	–	–	7.8	244.8	3.5	16:24	12.5
5149*	75.3	1	–	–	–	3.6	304.5	0.3	16:18	12.9
5153	73.5	4	0.5	1.1	78	−0.2	264.1	5.0	16:18	13.4
5159	71.1	1	–	–	–	−6.9	24.1	1.4	16:24	14.3
5167	76.0	2	0.4	0.5	60	3.1	303.5	0.6	16:12	15.3
5177*	72.0	1	–	–	–	−10.2	23.5	1.2	16:18	16.7
5196	71.0	3	0.3	0.4	60	−5.3	281.9	5.2	15:54	19.3
5201	69.7	2	3.0	4.3	83	−1.2	142.0	−3.5	15:54	19.9
5206*	74.7	3	0.4	0.7	90	5.4	1.7	2.2	15:54	20.6
5207	80.7	1	–	–	85	6.8	261.7	4.7	15:48	20.7
5208	66.4	3	1.3	2.2	68	−10.0	161.0	−2.8	15:48	20.9
5279	77.8	2	1.0	1.5	63	0.5	257.1	6.4	15:06	30.3

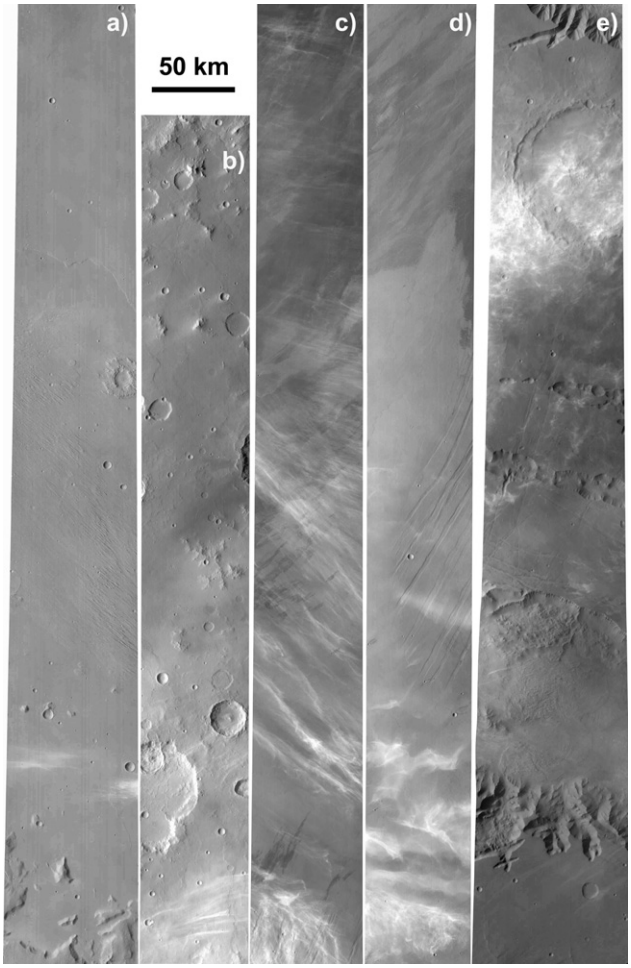

Fig. 4. CO_2 ice cloud examples in the HRSC blue band, all images contrast enhanced and map-projected to Mars IAU reference ellipsoid: (a) orbit 5201, Aeolis Mensae (S of Elysium, 149°E, Ls 19.9°); (b) orbit 5149, Xanthe Terra (304.5°E, Ls 12.9°, CO_2 ice identified by OMEGA); (c) orbit 5153, Tharsis Planitia (Fortuna Fossae, 264.1°E, Ls 13.4°); (d) orbit 5117, Tharsis Planitia (Fortuna Fossae, 265.9°E, Ls 8.5°); (e) orbit 5196, Valles Marineris (Tithoniae Catena, 281.9°E, Ls 19.3°).

overview of the cloud morphologies and examples are shown in Fig. 4. The prevailing form is a ripple-like elongated habit oriented roughly in E–W, sometimes NW–SE directions. We have encountered solitary clouds (Fig. 4a), cloud groups (Fig. 4b) as well as extended fields of clouds spread over more than 10° in latitude (Fig. 4c and d). There are several examples of ripple-like cloud forms occurring together with cloud patches like in Fig. 1. Orbit 5196 (Fig. 4e) exhibits a more clumpy form but the high spatial resolution of HRSC reveals a mainly filamentary interior structure of the cloud. While Montmessin et al. (2007) described the predominance of clumpy (convective, cumulus-type) cloud morphologies, our observations demonstrate that ripple-like and filament forms are more frequent than previously thought. The occurrence of waves and a multitude of morphologies points to different phenomena and formation mechanisms dictated by atmospheric dynamics and microphysical constraints. However, these aspects can be fully explored only with future modelling studies.

4.3. CO_2 ice cloud distribution

In the period of about 3 months after northern spring equinox of Martian year 29 HRSC and OMEGA together have detected mesospheric CO_2 ice clouds in 40 orbits. Cloud occurrences observed by both instruments are mainly confined to a latitudinal belt of $\pm 20°$ around the equator with all HRSC detections within $\pm 12°$ latitude. A similar restriction in latitudes of high-altitude clouds in northern spring was observed by TES/MOC on MGS during the three Martian years 24–26 and Clancy et al. (2007) proposed the term Martian Equatorial Mesospheric clouds (MEM) for this type of clouds. The geographic and seasonal distributions of our observations are depicted in Fig. 5. CO_2 ice clouds appear very early in spring at Ls=0.8° (orbit 5062, 11 December 2007) and were detected for the last time by OMEGA in orbit 5321 at Ls=35.7°. There were no other mesospheric cloud detections throughout the entire northern spring. This differs from observations in previous Martian years by OMEGA (Montmessin et al., 2007), by SPICAM (Montmessin et al., 2006) and by TES/MOC (Clancy et al., 2007) where the equatorial CO_2 ice clouds were encountered mainly in spring between Ls 0° and Ls 55°. Mesospheric cloud frequencies, however, change over the years indicating quite some interannual variability. In Martian year 28 there were almost no equatorial CO_2 ice cloud detections at all which may partially be related to an observational bias effect (Määttänen et al., 2008). Clouds were not observed prior to Ls 20° in Martian year 27. Most of the CO_2 ice clouds are found at longitudes between 240°E and 30°E which is consistent with former observations. There are especially two regions where

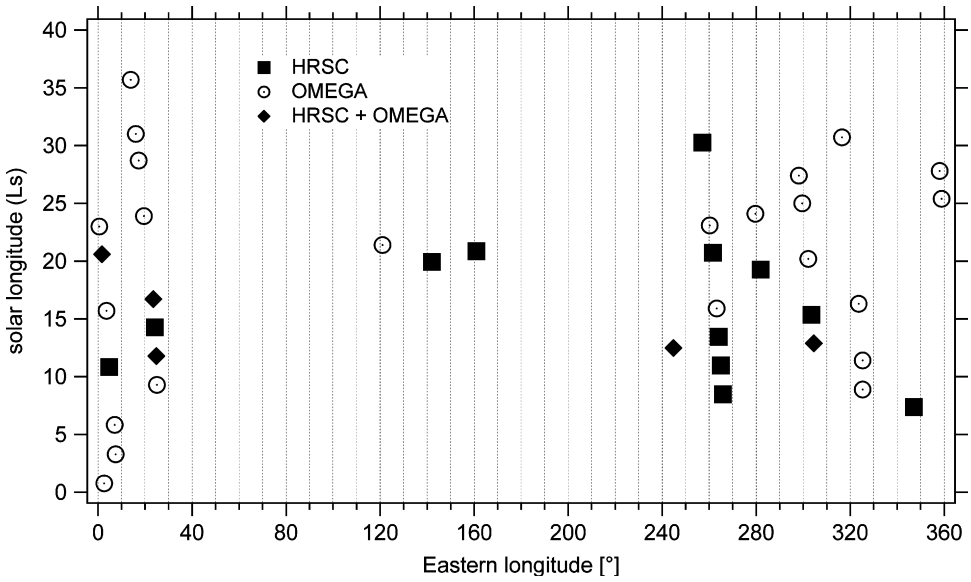

Fig. 5. Longitudinal and seasonal distribution of the equatorial mesospheric CO_2 ice clouds from 11 December 2007 until 23 February 2008 (Martian year 29) detected by MEx HRSC and OMEGA experiments.

mesospheric clouds have been observed for more than a month whenever one of the two instruments was switched-on. In Sinus Meridiani at about 0°E CO_2 ice clouds were detected 9 times within 57 days, at about 20°E mesospheric clouds were observed 8 times within 58 days and in Tharsis Planitia at about 260°E clouds occurred 7 times within 45 days (cp. Fig. 5). In the western hemisphere, we found mesospheric clouds only three times and all of them at about Ls 20° despite numerous other observations in the same areas. This limited longitudinal distribution points towards local mechanisms driving the cloud formation: cold enough temperatures are attained only in certain locations, possibly through interplay between the general circulation and local disturbances, such as gravity waves.

5. Conclusion and outlook

This paper summarizes mesospheric cloud observations in early Northern spring performed by the HRSC and OMEGA experiments during the third Martian year of Mars Express. HRSC shows cloud features in its green and blue channels. The small along-track stereo angle between these sensors allows for the determination of the altitude of single features with an absolute accuracy of 1–2 km and an additional 0.7 km uncertainty for each 10 m/s along-track (North–South) movement. This accuracy has been verified by measurements within 17 HRSC data sets. In addition, the time delay between data from both sensors allows for the determination of across-track (East–West) velocity components with an accuracy of about 10–13 m/s. The measurement results locate cloud features in altitudes of 66–83 km with a mean of 75 km. The detected East–West velocity range is 60–93 m/s with a mean of 73 m/s. When OMEGA was operating in parallel, the spectral CO_2 ice signatures around 4.26 μm could clearly be related to the HRSC measurements.

The two instruments onboard Mars Express encountered high-altitude CO_2 ice clouds in 40 orbits during a period in Martian year 29 covering Ls 0° to Ls 36°. Nearly all detections occur within an area ranging from the Tharsis region to Sinus Meridiani at longitudes between 240°E and 30°E and at latitudes below 20° around the equator. The prevailing cloud morphologies as revealed by HRSC imagery are ripple-like or filamentary forms and modelling studies are needed to better understand the processes involved in the formation and dissipation of mesospheric clouds.

An inventory of all HRSC data sets is planned in order to survey the altitude, vertical structures, and other parameters of all apparent cloud-like features. It will include CO_2 ice clouds as well as already observed low-altitude features, ranging from 0 to 20 km and most probably linked to H_2O ice clouds. We expect that the statistics of the aspired data base might allow to better constrain and to derive rules for modelling, whether and how far the occurrence of the cloud phenomena depend on the geographic location and/or on seasonal and local time parameters.

Acknowledgements

The authors appreciate the efforts from the HRSC and OMEGA experiments and science teams in making both experiments a (ongoing) success. We would also like to thank all personnel involved at ESTEC, ESOC and ESAC to have the Mars Express mission operating in orbit around Mars. We further appreciate the comments and suggestions by two anonymous reviewers which helped to improve our manuscript. AM acknowledges funding from the Centre National d'Études Spatiales (CNES).

References

Angelats i Coll, M., Forget, F., López-Valverde, M.A., González-Galindo, F., 2005. The first Mars thermospheric general circulation model: the Martian atmosphere from the ground to 240 km. Geophys. Res. Lett. 32, L04201, doi:10.1029/2004GL021368.

Bibring, J.-P. et al., 2004. OMEGA: Observatoire pour la Minéralogie, l'Eau, les Glaces et l'Activité. In: Mars Express: The scientific payload, Eur. Space Agency Spec. Publ., ESA-SP 1240, pp. 37–50.

Bibring, J.-P., Langevin, Y., Gendrin, A., Gondet, B., Poulet, F., Berthé, M., Soufflot, A., Arvidson, R., Mangold, N., Mustard, J., Drossart, P., et al., 2005. Mars surface diversity as revealed by the OMEGA/Mars Express observations. Science 307, 1576–1581.

Clancy, R.T., Sandor, B.J., 1998. CO_2 ice clouds in the upper atmosphere of Mars. Geophys. Res. Lett. 25, 489–492.

Clancy, R.T., Grossman, A.W., Wolff, M.J., James, P.B., Rudy, D.J., Billawala, Y.N., Sandor, B.J., Lee, S.W., Muhleman, D.O., 1996. Water vapour saturation at low altitudes around Mars aphelion: a key to Mars climate? Icarus 122, 36–62.

Clancy, R.T., Wolff, M.J., Whitney, B.A., Cantor, B.A., Smith, M.D., 2007. Mars equatorial mesospheric clouds: global occurrence and physical properties from Mars Global Surveyor Thermal Emission Spectrometer and Mars Orbiter Camera limb observations. J. Geophys. Res. 112, E04004, doi:10.1029/2006JE002805.

Colaprete, A., Barnes, J.R., Haberle, R.M., Montmessin, F., 2008. CO_2 clouds, CAPE and convection on Mars: observations and general circulation modelling. Planet. Space Sci. 56, 150–180.

Fedorova, A.A., Korablev, O.I., Bertaux, J.-L., Rodin, A.V., Montmessin, F., Belyaev, D.A., Rébérac, A., 2009. Solar infrared occultation observations by SPICAM experiment on Mars Express: simultaneous measurements of the vertical distributions of H_2O, CO_2 and aerosol. Icarus 200, 96–117.

Forget, F., Hourdin, F., Fournier, R., Hourdin, C., Talagrand, O., Collins, M., Lewis, S.R., Read, P.L., Huot, J.-P., 1999. Improved general circulation models of the Martian atmosphere from the surface to above 80 km. J. Geophys. Res. 104, 24155–24176.

Forget, F., Montmessin, F., Bertaux, J.-L., González-Galindo, F., Lebonnois, S., Quémerais, E., Reberac, A., Dimarellis, E., López-Valverde, M.A., 2009. The density and temperatures of the upper Martian atmosphere measured by stellar occultations with Mars Express SPICAM. J. Geophys. Res. 114, E01004, doi:10.1029/2008JE003086.

Formisano, V., Maturilli, A., Giuranna, M., D'Aversa, E., Lopez-Valverde, M.A., 2006. Observations of non-LTE emission at 4–5 microns with the planetary Fourier spectrometer aboard the Mars Express mission. Icarus 182, 51–67.

Gwinner, K., Scholten, F., Spiegel, M., Schmidt, R., Giese, B., Oberst, J., Heipke, C., Jaumann, R., Neukum, G., 2009a. Derivation and validation of high-resolution digital terrain models from Mars Express HRSC-data. Photogramm. Eng. Remote Sensing 75 (9), 1127–1142.

Gwinner, K., Scholten, F., Preusker, F., Elgner, S., Roatsch, T., Spiegel, M., Schmidt, R., Oberst, J., Jaumann, R., Heipke, C., 2009b. Topography of Mars from global mapping by HRSC high-resolution digital terrain models and orthoimages: characteristics and performance. Earth Planet. Sci. Lett., in press, doi:10.1016/j.epsl.2009.11.007.

Inada, A., Richardson, M.I., McConnochie, T.H., Strausberg, M.J., Wang, H., Bell, J.F., 2007. High-resolution atmospheric observations by the Mars Odyssey Thermal Emission Imaging System. Icarus 192, 378–395.

Ivanov, A.B., Muhleman, D.O., 2001. Cloud reflection observations: results from the Mars Orbiter Laser Altimeter. Icarus 154, 190–206.

James, P.B., Kieffer, H.H., Paige, D.A., 1992. The seasonal behaviour of water on Mars. In: Kieffer, H.H. (Ed.), Mars. University of Arizona Press, Tucson, pp. 934–968.

Jaumann, R., Neukum, G., Behnke, T., Duxbury, T., Eichentopf, K., Flohrer, J.v, Gasselt, S., Giese, B., Gwinner, K., Hauber, E., Hoffmann, H., Hoffmeister, A., Köhler, U., Matz, K.-D., McCord, T.B., Mertens, V., Oberst, J., Pischel, R., Reiss, D., Ress, E., Roatsch, T., Saiger, P., Scholten, F., Schwarz, G., Stephan, K., Wählisch, M., et al., 2007. The high-resolution stereo camera (HRSC) experiment on Mars Express: instrument aspects and experiment conduct from interplanetary cruise through the nominal mission. Planet. Space Sci. 55, 928–952.

Joshi, M.M., Lawrence, B.N., Lewis, S.R., 1995. Gravity wave drag in three-dimensional atmospheric models of Mars. J. Geophys. Res. 100, 21235–21246.

Lellouch, E., Rosenqvist, J., Goldstein, J.J., Bougher, S.W., Paubert, G., 1991. First absolute wind measurements in the middle atmosphere of Mars. Astrophys. J. 383, 401–406.

Määttänen, A., Montmessin, F., Gondet, B., Hoffmann, H., Scholten, F., Hauber, E., Bibring, J.-P., Neukum, G., 2008. Equatorial CO_2 clouds on Mars: OMEGA and HRSC data analysis. (Abstract) Paper presented at Workshop Mars Atmosphere: Modelling and Observations (2008), Williamsburg, USA, LPI 9005.pdf.

Määttänen, A., Montmessin, F., Gondet, B., Scholten, F., Hoffmann, H., Hauber, E., González-Galindo, F., Spiga, A., Forget, F., Neukum, G. , Bibring, J.-P., Bertaux, J.-L. Mapping the properties of the mesospheric CO_2 clouds observed by Mars Express: OMEGA and HRSC observations and a comparison to the LMD-MGCM. Icarus, submitted for publication.

McConnochie, T.H., Bell, J.F., Savransky, D., Wolff, M.J., Christensen, P.R., Richardson, M.I., Titus, T.N., 2005. THEMIS-VIS measurements of the altitude and velocity of clouds in the Martian mesosphere. (Abstract) Paper presented at AGU 2005 Fall Meeting, USA, P21–E03.

McConnochie, T.H., Smith, M.D., 2008. Vertically resolved aerosol climatology from Mars: Global Surveyor Thermal Emission Spectrometer (MGS-TES) limb sounding. (Abstract) Paper presented at Workshop Mars Atmosphere: Modelling and Observations (2008), Williamsburg, USA, LPI 9114.pdf.

McConnochie, T.H., Bell, J.F., Savransky, D., Mehall, G., Caplinger, M., Christensen, P.R., Cherednik, L., Bender, K., Dombovari, A., 2006. Calibration and in-flight performance of the Mars Odyssey Thermal Emission Imaging System Visible Imaging Subsystem (THEMIS-VIS). J. Geophys. Res. 111 (E10), 6018.

McConnochie, T.H., Bell, J.F., Savransky, D., Wolff, M.J., Toigo, A.D., Wang, H., Richardson, M.I., Christensen, P.R. THEMIS-VIS observations of clouds in the Martian mesosphere: altitudes, wind speeds, and decameter-scale morphology, Icarus, submitted for publication.

Montmessin, F., Bertaux, J.-L., Quémerais, E., Korablev, O., Rannou, P., Forget, F., Perrier, S., Fussen, D., Lebonnois, S., Rébérac, A., Dimarellis, E., 2006. Subvisible CO_2 ice clouds detected in the mesosphere of Mars. Icarus 183, 403–410.

Montmessin, F., Gondet, B., Bibring, J.-P., Langevin, Y., Drossart, P., Forget, F., Fouchet, T., 2007. Hyper-spectral imaging of convective CO_2 ice clouds in the equatorial mesosphere of Mars. J. Geophys. Res. 112, E11S90, doi:10.1029/2007JE002944.

Moreno, R., Lellouch, E., Forget, F., Encrenaz, T., Guilloteau, S., Millour, E., 2009. Wind measurements in Mars' middle atmosphere: IRAM Plateau de Bure interferometric CO observations. Icarus 201, 549–563, doi:10.1016/j.icarus.2009.01.027.

Neukum, G., Jaumann, R., the HRSC Co-investigator and Experiment Team, 2004. HRSC: the High Resolution Stereo Camera of Mars Express. In: Mars Express: The scientific payload, Eur. Space Agency Spec. Publ., ESA-SP 1240, pp. 17–35.

Pettengill, G.H., Ford, P.G., 2000. Winter clouds over the north Martian polar cap. Geophys. Res. Lett. 27, 609–612.

Rodin, A.V., Korablev, O.I., Moroz, V.I., 1997. Vertical distribution of water in the near-equatorial troposphere of Mars: water vapour and clouds. Icarus 125, 212–229.

Schofield, J.T., Crisp, D., Barnes, J.R., Haberle, R.M., Magalhães, J.A., Murphy, J.R., Seiff, A., Larsen, S., Wilson, G., 1997. The Mars Pathfinder atmospheric structure investigation/meteorology (ASI/MET) experiment. Science 278, 1752–1757.

Scholten, F., Gwinner, K., Roatsch, T., Matz, K.-D., Wählisch, M., Giese, B., Oberst, J., Jaumann, R., Neukum, G., et al., 2005. Mars Express HRSC data processing—methods and operational aspects. Photogramm. Eng. Remote Sensing 71, 1143–1152.

Sonnabend, G., Sornig, M., Krötz, P.J., Schieder, R.T., Fast, K.E., 2006. High spatial resolution mapping of Mars mesospheric zonal winds by infrared heterodyne spectroscopy of CO_2. Geophys. Res. Lett. 33, L18201, doi:10.1029/2006GL026900.

Sonnabend, G., Sornig, M., Krötz, P.J., Stupar, D., Montabone, L., Fast. K.E., Schieder, R.T., 2008. Mars mesospheric winds around Northern spring equinox from high resolution infrared spectroscopy. (Abstract) Paper presented at Workshop Mars Atmosphere: Modelling and Observations (2008), Williamsburg, USA, LPI 9055.pdf.